Biochimica et Biophysica Acta 1848 (2015) 1285–1293

Contents lists available at ScienceDirect

Biochimica et Biophysica Acta

journal homepage: www.elsevier.com/locate/bbamem

Structure and membrane interactions of chionodracine, a piscidin-like antimicrobial peptide from the icefish *Chionodraco hamatus*

Cristina Olivieri [a], Francesco Buonocore [a], Simona Picchietti [a], Anna Rita Taddei [d], Chiara Bernini [a], Giuseppe Scapigliati [a], Alysha A. Dicke [b,c], Vitaly V. Vostrikov [b,c], Gianluigi Veglia [b,c,*], Fernando Porcelli [a,**]

[a] Department for Innovation in Biological, Agro-food, and Forest Systems, University of Tuscia, Viterbo 01100, Italy
[b] Department of Biochemistry, Molecular Biology and Biophysics, University of Minnesota, Minneapolis 55455, USA
[c] Department of Chemistry, University of Minnesota, Minneapolis 55455, USA
[d] Section of Electron Microscopy, Great Equipment Center, University of Tuscia, Viterbo 01100, Italy

ARTICLE INFO

Article history:
Received 11 December 2014
Received in revised form 23 February 2015
Accepted 27 February 2015
Available online 6 March 2015

Keywords:
Piscidins
Antimicrobial peptides
Fluorescence
NMR
Membrane permeabilization
Structure

ABSTRACT

Chionodracine (Cnd) is a 22-residue peptide of the piscidin family expressed in the gills of the *Chionodraco hamatus* as protection from bacterial infections. Here, we report the effects of synthetic Cnd on both *Psychrobacter* sp. TAD1 and *Escherichia coli* bacteria, as well as membrane models. We found that Cnd perforates the inner and outer membranes of *Psychrobacter* sp. TAD1, making discrete pores that cause the cellular content to leak out. Membrane disruption studies using intrinsic and extrinsic fluorescence spectroscopy revealed that Cnd behaves similarly to other piscidins, with comparable membrane partition coefficients. Membrane accessibility assays and structural studies using NMR in detergent micelles show that Cnd adopts a canonical topology of antimicrobial helical peptides, with the hydrophobic face toward the lipid environment and the hydrophilic face toward the bulk solvent. The analysis of Cnd free energy of binding to vesicles with different lipid contents indicates a preference for charged phospholipids and a more marked binding to native *E. coli* extracts. Taken with previous studies on piscidin-like peptides, we conclude that Cnd first adsorbs to the membrane, and then forms pores together with membrane fragmentation. Since Cnd has only marginal hemolytic activity, it constitutes a good template for developing new antimicrobial agents.

1. Introduction

Antimicrobial peptides (AMPs) represent an ancestral eukaryotic mechanism of immunity against prokaryotic organisms [1–3]. In particular, fish express a large variety of antimicrobial peptides, such as defensins, cathelicidins, hepcidins and piscidins [4–6]. Fish AMPs such as piscidin-2 act as anti-infective agents, and display high potency against human and fish pathogens [7], while other peptides, such as epinecidin-1, show anticancer activity against human fibrosarcoma cells [8].

Among the fish AMPs, piscidins constitute a rather interesting family. They are histidine- and phenylalanine-rich peptides with a broad spectrum of antimicrobial activity, and are effective against viruses, fungi and bacteria [7]. Three isoforms of piscidin have been isolated from the fish mast cells (i.e., piscidins 1, 2, and 3), differing by one or two residues [9]. Also, a new type of piscidin (i.e., piscidin 4) comprising 44 residues has been isolated and characterized from hybrid striped bass [10]. Interestingly, piscidins display in vitro anti-tumor activity against various cancer cell lines, such as HL60, HeLa [11], MCF7, and 4T1 [12]. While the activity of piscidins has been attributed to their ability to form pores and disrupt cell membranes, they also have immunomodulatory properties, suggesting that they may target specific receptors [13,14]. Other reports show that piscidins may also inhibit the biosynthesis of the cell wall, nucleic acids, and proteins, or, alternatively inhibit pathogens' enzymatic activity [5].

We recently discovered a new antimicrobial peptide of the piscidin family named chionodracine (Cnd), which is produced by *Chionodraco hamatus*, an Antarctic teleost icefish, of the Channichthyidae family [4]. Cnd protects *Chionodraco* from infections; specifically, from the attack of *Psychrobacter* sp. TAD1 and TA144, two psychrotolerant and psychrophilic bacteria strains typical of the Antarctic marine and terrestrial environments [4]. Cnd is expressed in the gills and head kidney of the *Chionodraco* as an 80 amino acid precursor and cleaved into a mature 22-residue peptide (*FFGHLYRGITSVVKHVHGLLSG*). We found that Cnd is active toward both *Psychrobacter* sp. TAD1 and TA144, but also shows activity toward Gram-positive *Bacillus cereus* and Gram-negative *Escherichia coli*. The minimum inhibitory concentrations (MIC) of the Cnd against mesophilic and psychrophilic bacteria have been previously reported and range between 5.00 and 20 μM [4]. Importantly, Cnd does not show any significant hemolytic activity toward

* Corresponding author. Tel.: +1 612 625 0758.
** Corresponding author. Tel.: +39 0761357041.
E-mail addresses: vegli001@umn.edu (G. Veglia), porcelli@unitus.it (F. Porcelli).

http://dx.doi.org/10.1016/j.bbamem.2015.02.030
0005-2736/

human erythrocytes, with a ~0.8% percentage of hemolysis at 50 μM [4], making it a promising template to develop new molecules with antimicrobial activity. Cnd's primary sequence is remarkably similar to that of other peptides belonging to the piscidin family, sharing the two N-terminal phenylalanines, the central glycine, and three histidines (Fig. 1). Although we have described the gene sequence, localization as well as the bactericidal activity of Cnd, we had yet to determine its interactions with prokaryotic cell membranes as well as the molecular and structural features of this peptide in membrane mimetic environments.

Here, we report the membranolytic properties and structural characterization of Cnd using transmission electron microscopy (TEM), cell permeation assays, and NMR spectroscopy. We found that Cnd interacts with cell membranes, disrupting the inner and outer membranes of both *Psychrobacter* sp. TAD1 and *E. coli* bacteria. In particular, TEM images reveal that Cnd forms well-defined pores in the bacterial membranes. Moreover, experiments carried out with synthetic membranes reveal a small but significant preference for negatively charged lipid membranes and a more marked affinity for *E. coli* bacteria membranes. The three-dimensional structure of Cnd is very similar to that of the piscidin-1 peptide, adopting a canonical amphipathic helix, with hydrophobic amino acids adsorbed on the membrane surface and the hydrophilic amino acids pointing toward the bulk solvent. Taken together, the helical propensity (disorder to order transition), membrane binding assays, and TEM images show the formation of discrete pores as well as membrane fragmentation that enable the cellular content to leak out and killing the cells.

2. Material and methods

2.1. Peptide synthesis

The Cnd peptide (>95%) *FFGHLYRGITSVVKHVHGLLSG* was purchased from United Biosystems Inc., USA. Peptide concentration was determined by light absorption at 280 nm before each sample preparation.

2.2. Lipid vesicle preparation

LUVs (Large Unilamellar Vesicles) of the appropriate lipid or lipid mix suspension were prepared by extrusion with an Avanti Polar mini-extruder through a polycarbonate membrane with pore sizes of 100 nm. Lipid vesicles were composed of 1-palmitoyl-2-oleoyl-sn-glycero-3-phosphocholine (POPC), mixtures of POPC and 1-palmitoyl-2-oleoyl-sn-glycero-3-phosphoglyceol (POPG), or *E. coli* B extract, ATCC 11303, comprised of 57.5% PE, 15.1% PG, 9.8% cardiolipin (CA), and 17.6% unknown (Avanti Polar Lipids Inc.). All the lipid vesicles were prepared as reported in the following sections.

2.3. Transmission Electron Microscopy (TEM)

Psychrobacter sp. TAD1 Antarctic bacteria were grown aerobically and cultured at 15 °C for 48 h in Luria–Bertani broth to mid-log phase (OD 600 of 0.35), centrifuged at 3000 *g* for 10 min at 25 °C, washed and resuspended into 10 mM Tris–HCl (pH 7.4), and 150 mM NaCl (working buffer) to a final OD600 of 0.5. Treated cells were incubated with Cnd antimicrobial peptide (15 μM, PM 2424.83) while control cells were maintained in working buffer, all the groups of cells were then collected at 0, 10 and 180 min and fixed with 2% paraformaldehyde + 2.5% glutaraldehyde in cacodylate sucrose buffer (0.1 M cacodylate, 0.09 M sucrose, 0.01 M $CaCl_2$, 0.01 M $MgCl_2$, pH 6.9) containing 0.075% ruthenium red and 0.075 M lysine acetate for 20 min at 4 °C. Samples were washed in cacodylate sucrose buffer containing 0.075% ruthenium red and then fixed with 2% paraformaldehyde + 2.5% glutaraldehyde in cacodylate sucrose buffer containing 0.075% ruthenium red overnight at 4 °C. After washings in the cacodylate sucrose buffer containing 0.075% ruthenium red, samples were post-fixed in 1% OsO4 + 0.075% ruthenium red in 0.1 M cacodylate buffer at pH 7.2 for 1 h at room temperature and then washed again in the cacodylate sucrose buffer containing 0.075% ruthenium red. Specimens were dehydrated in a graded ethanol series and embedded in LR White resin (Multilab Supplies, Surrey, England) [15]. The resin was polymerised in tightly capped gelatine capsules for 48 h at 50 °C. Thin sections were cut with Reichert Ultracut and LKB Nova ultramicrotomes using a diamond knife, collected on copper grids, stained with uranyl acetate and lead citrate, and observed with a JEOL 1200 EX II electron microscope at 100 kV. Micrographs were acquired by the Olympus SIS VELETA CCD camera equipped the iTEM software. TEM images (at the same magnification) were analysed to determine the percentage of damaged bacteria (bacteria with destroyed membranes) both in controls and treated cells, by counting a total number of 50,000 cells. All the numerical results are presented in the text as mean ± SD. Homogeneity of variances was tested before data processing. To detail the source of variation attributed to treatment and time factors, two-way ANOVA was applied, followed by Bonferroni's test. Data were analysed using the GraphPad Prism 3.0 software statistical package. The level for accepted statistical significance was $P < 0.01$.

```
Chionodracine   FFGHLYRGITSVVKHVHGLLSG
Piscidin 1      FFHHIFRGIVHVGKTIHRLVTG
                FFHHIFRGIVHVGKTIHRLVTG
Piscidin 2      FFHHIFRGIVHVGKTIHKLVTG
Piscidin 3      FIHHIFRGIVHAGRSIGRFLTG
Piscidin 4      FFRHLFRGAKAIFRGARQGXRAHKVVSRYRNRDVPETDNNQEEP
```

Fig. 1. Primary sequences for Cnd and other piscidin antimicrobial peptides with sequence homology highlighted.

2.4. Steady-state fluorescence experiments

2.4.1. Partition studies

A Perkin Elmer LS55 steady-state fluorescence spectrometer was used for steady-state fluorescence measurements. The experiments were carried out at 25 °C in a thermostated cell holder equipped with magnetic stirrer. In order to correct for polarization effects and reduce direct contributions from the vesicles, light scattering measurements were carried out with a cross-oriented configuration of polarizers ($Pol_{em} = 0°$ and $Pol_{exc} = 90°$) [16]. The partition of Cnd with lipid vesicles was quantified by titrating the peptide samples in 20 mM phosphate buffer at pH 7.4 containing EDTA 0.8 mM and NaCl 150 mM with increasing amounts of vesicle stock solutions; the lipid/peptide ratio ranged from 50 to 500. These binding assays were repeated with LUVs of different compositions: 100% POPC, 70%/30% POPC/POPG, and *E. coli* B extract. The lipid titrations were monitored following the increase of Tyr-6 fluorescence at $\lambda_{em} = 320$ nm upon excitation at $\lambda_{exc} = 274$. The background signals of both buffer and lipid vesicles were subtracted from each spectrum. The partition constant K_x, was defined according to Wimley and White [17,18]:

$$K_x = \frac{[P]_{bil}/[L]}{[P]_{water}/[W]}$$

where $[P]_{bil}$ and $[P]_{water}$ are the bulk molar concentration of peptide in the bilayer and in the water, and $[L]$ and $[W]$ are the molar concentrations of lipid and water, respectively. The partition constants were measured by titrating a 1 μM solution of Cnd with increasing amounts of lipid vesicles of varying compositions, then calculating the fraction of the peptide, f_p, partitioned into the lipid vesicles. Considering that $[P]_{tot} = [P]_{water} + [P]_{bil}$ [19,20], the expression for f_p is:

$$f_x = \frac{K_x[L]}{[W] + K_x[L]}.$$

The values of K_x were determined by the plot of f_p vs *[L]* using the GraphPad Prism 6 software package (GraphPad Software Inc.). Experimental data were fitted using equation [19]:

$$\frac{F}{F_o} = 1 + (F_{max} - 1) f_p$$

where F is the fluorescence intensity, F_o and F_{max} are the fluorescence intensities before lipid vesicle addition and at saturation, respectively. In order to avoid the non-ideal behavior occurring at higher concentrations [18,21], the molar partition coefficients were evaluated at a low peptide concentration (~1 μM).

2.4.2. Outer membrane disruption assay

For cell permeabilization studies, we used ANS (1-aminonaphtalene-8-sulfonic acid) uptake assays [22] with *E. coli* BL21(DE3) and *Psychrobacter* sp. TDA1 bacteria. Bacterial cells were cultured in LB medium. Cells from the mid-log phase were centrifuged, washed, and then resuspended in PBS buffer to achieve an OD_{600} of ~1.2. Increasing amounts of peptide (ranging from 1.0 to 15.0 μM) were added to 1.0 mL of cell suspension in the presence of 5.0 μM of ANS. The spectra were recorded between 400 and 600 nm with an excitation wavelength of 360 nm and excitation/emission band-passes of 5.0 nm. The disruption of the outer membrane was quantified by the increase in fluorescence intensity and the blue shift of the spectra.

2.4.3. Calcein leakage studies

The kinetics of calcein release were followed by monitoring the fluorescence increase upon peptide binding to vesicles at different lipid compositions. LUVs charged with 50 mM calcein were prepared by an extrusion process. Briefly, the appropriate amount of lipids was dissolved in chloroform in a small round bottom flask and the solvent was gently removed in a rotary evaporator. The remaining solvent was removed under vacuum overnight at room temperature. The dried lipid films were hydrated with MOPS buffer at pH 7.5 containing 70 mM NaCl, E0.8 mM DTA, and 50 mM calcein. The lipid suspensions were vortexed at room temperature and subjected to 5 freezing and thawing cycles. After freezing, the sample was heated to 50 °C and the mixture subjected to extrusion cycles using an Avanti polar mini-extruder containing two stacked 100 nm polycarbonate filters. To separate the non-encapsulated calcein in the external medium, the mixture was passed through a Sephadex-G50 column. Columns containing the calcein-loaded vesicles were centrifuged for 3 min at 1000 rpm. The lipid concentration was measured via the static light scattering at 90° of the lipid suspension at 550 nm and compared with a calibration curve [23]. The Bartlett method was used to determine the total phospholipid concentration. Fluorescence studies were carried out at 25 °C with an excitation wavelength of 490 nm, producing an emission wavelength of 520 nm. The excitation and emission band-passes were 2.5 nm. LUVs charged with 50 mM calcein showed very little fluorescence quantum yield due to calcein self-quenching. The increase in observed fluorescence was due to the vesicle leakage caused by peptide addition. Before peptide titration (from 0.1 to 1.0 μM), the fluorescence baseline was monitored for 5 min and no deviations were observed. After peptide addition, the fluorescence was monitored up to 2000 s. To obtain the maximal leakage of the vesicles and normalize fluorescence intensities, we added ~5 μL of 0.1% solution of Triton X to each sample. Before each measurement, we performed light scattering experiments between 540 and 560 nm to assess the integrity of the vesicles [23]. Fluorescence traces were fitted with a double exponential equation [23]

$$F_t = F_{eq} - a_1 e^{-k_1 t} - a_2 e^{-k_2 t}$$

where F_t and F_{eq} are the fluorescence at time t and at $t \rightarrow \infty$,respectively, the constants a_1 and a_2 represent the fractions of the two kinetic components and k_1 and k_2 are the respective constants expressed in s^{-1}. The percentage of calcein release was calculated using the formula:

$$Dye\,release(\%) = \frac{F - F_0}{F_t - F_0}$$

where F is the fluorescence upon addition of peptide, F_0 is the initial fluorescence before the addition of peptide and F_t is the fluorescence upon addition of Triton-X.

2.4.4. Iodide quenching experiments

Quenching of the tyrosine fluorescence both in the presence and absence of lipid vesicles was measured by addition of increasing aliquots of potassium iodide [24]. The excitation wavelength was set to 274 nm and florescence spectra were recorded between 295 and 360 nm. Fluorescence spectra were corrected for dilution and for the absorption of fluorophores and quenchers. The data were fitted according to the Stern–Volmer equation:

$$\frac{F_o}{F} = 1 + K_{SV}[Q]$$

where F_o and F are the fluorescence in the absence and presence of the quencher Q, respectively, and K_{SV} is the Stern–Volmer constant accounting for the collisional quenching process [25].

2.5. NMR sample preparation and spectroscopy

The lyophilized peptide was dissolved in an aqueous solution (5% ^2H_2O, 95% H_2O) containing 300 mM perdeuterated DPC (Cambridge Isotope Laboratories) and 20 mM phosphate buffer at pH ~6.5 to a final concentration of ~1.5 mM. All of the NMR experiments were acquired at 300 K on a Varian Inova 900 MHz spectrometer. The 2D [^{1}H, ^{1}H] total correlation spectroscopy (TOCSY) [26] (50 and 70 ms mixing time) and 2D [^{1}H, ^{1}H] NOESY [27] (70–300 ms mixing time) experiments were run in the phase-sensitive mode using time-proportional phase incrementation (TPPI) for quadrature detection in the indirect dimension. All of the pulse sequences utilized a WATERGATE pulse scheme [28] for solvent suppression. The experiments were acquired with 256 and 1024 complex data points in the t_1 and t_2 dimensions, respectively, with 64 scans per increment. The 90° pulse width was 30 kHz, and recycle delay was set to 1 s. A DIPSI-2 pulse sequence [29] was used for isotropic mixing in the 2D TOCSY experiments. The spectral widths were 5400 Hz t_1 and 7200 Hz t_2 dimensions. The 2D data were zero-filled to 8192 points in t_1 and to 4096 points in t_2 and then processed with a sine-bell squared window function shifted between 60° and 90° before Fourier transformation. A polynomial function was used for baseline correction in the direct frequency dimension. The NMR data were processed using *NMRPipe* [30] and analyzed with *SPARKY* [31] software packages. Proton dimension was referenced to the water line at 4.7 ppm. The spectra were assigned using the standard assignment approach described by Wuthrich [32]. [^{1}H,^{13}C] HSQC and HMBC spectra were acquired on a Bruker 900 MHz spectrometer at 30 °C. All the ^{13}C experiments were carried out at natural abundance. Analysis of the natural abundance of ^{13}C edited HSQC and HMBC has been used to resolve amino acid spin system assignments as well as provide $^{13}C_\alpha$ and $^{13}C_\beta$ chemical shifts. A table with all of the ^{1}H and ^{13}C chemical shift resonances is provided in the supporting information.

2.6. Structure calculations from NMR data

NOE cross-peaks from the 150 and 300 ms mixing time [^{1}H, ^{1}H]-NOESY experiments were integrated and used for the structure calculations. The NOE volumes were calibrated using the average NOE volume from resolved aromatic vicinal protons of Y6 and classified as strong, medium, and weak, corresponding to distance restraints of 1.8–2.9, 1.8–4.5, and 1.8–5.0 Å, respectively. *TALOS +* software [33] was used

to obtain the dihedral constraints for residues 3 through 19 that were then implemented in the structure calculations. The NMR conformers were calculated starting from an extended conformation of Cnd and minimized using a hybrid simulated annealing (SA) energy minimization protocol available in XPLOR-NIH [34]. A total of 100 conformers were generated using random seeds at an initial temperature of 5000 K with 6000 high temperature steps, 3000 cooling steps, and a step size of 5 fs. The final target function included a total of 240 NOEs (75 intra-residue and 165 inter-residue distances). The final stage of refinement of the structural ensemble was carried out starting at an initial temperature of 500 K and using 30,000 cooling steps with a 1 fs step size. The 70 refined structures had no NOE violations greater than 0.5 Å, no bond violations greater than 0.05 Å, and no bond angle violations greater than 4°. The 40 lowest energy conformers were then selected for further analysis. The analysis of Ramachandran angles for the 40 lowest energy structures was carried out using Molprobity [35]. For the final conformers, the occurrence of the ϕ and ψ angles for all of the residues in the Ramachandran plots was 83.6% in the most favored region, 11.1% in the allowed, 1.6% in the generously allowed, and 3.7% in disallowed regions. The residues located in the N- and C-termini, which had fewer structural restraints, account for those found in the disallowed regions of the Ramachandran plots.

3. Results

3.1. Effects of Cnd on the inner and outer membranes of Psychrobacter sp. TAD1 bacteria using transmission electron microscopy (TEM)

Examination of the *Psychrobacter* sp. TAD1 by TEM (Fig. 2A) revealed that the bacterium is bounded by two membranous structures. These two membranes, the inner membrane (IM) and the outer membrane (OM), are separated by a gel-like layer known as the periplasm

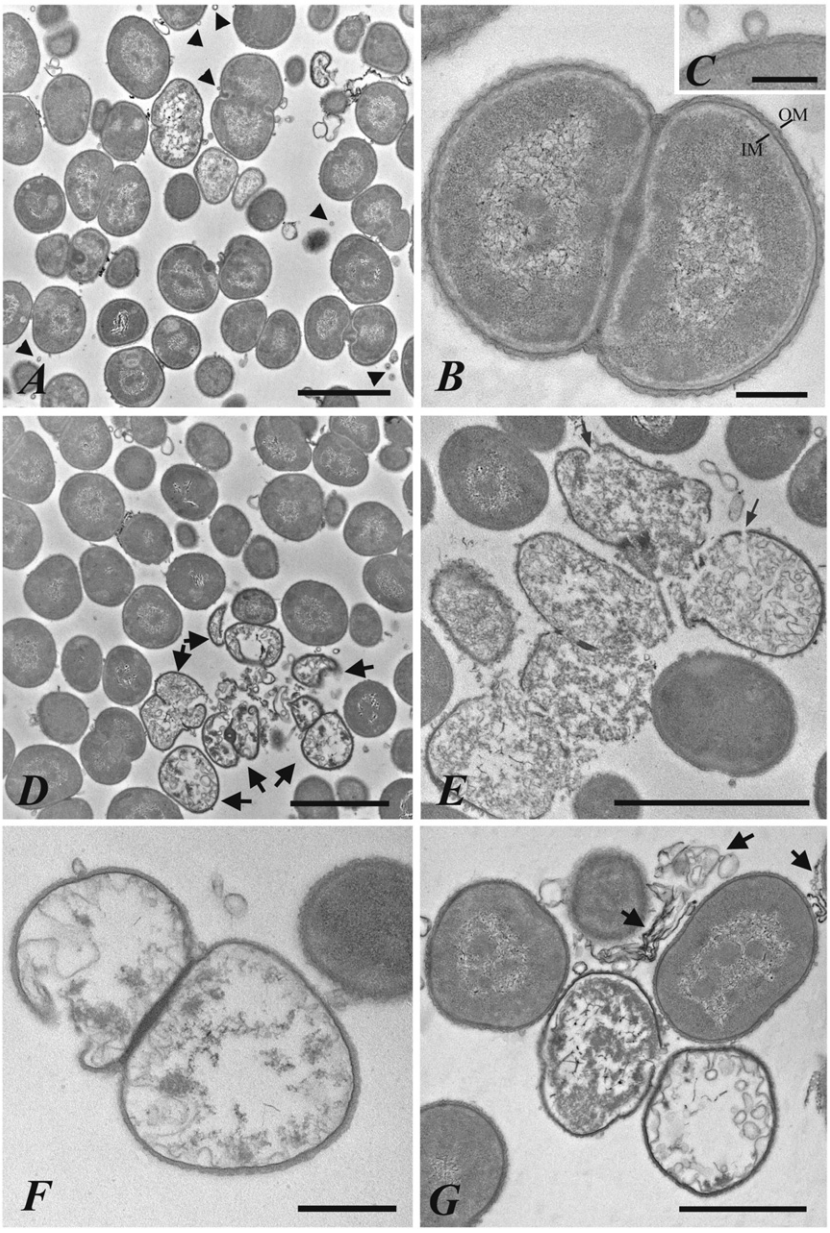

Fig. 2. TEM micrographs of ultrathin sections from *Psychrobacter* sp. TAD1. (A) General view of cells showing the OMVs interspersed among bacteria (arrow heads). (B) Magnified view of cells surrounded by two membranous structures: the inner membrane and the outer membrane. (C) Image showing the OMVs protruding from the bacterial outer membrane. (D) Bacteria showing membrane damage after 10 min of treatment (arrows). (E) Higher magnification of damaged bacteria showing discrete pores (arrows) together with membrane fragmentation. (F) Dividing cells with leakage of cellular contents after 10 min of treatment. (G) A detail of fragments of destroyed cellular membranes (arrows) after 10 min of treatment. IM: inner membrane; OM: outer membrane. Scale bar: 2 μm in (A); 250 nm in (B); 250 nm in (C); 2 μm in (D); 2 μm in (E); 500 nm in (F); 1 μm in (G).

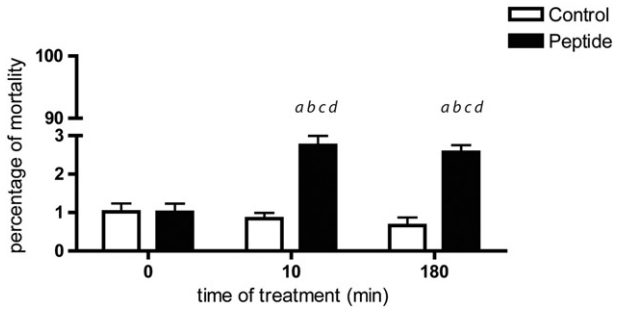

Fig. 3. Percentage of *Psychrobacter* sp. TAD1 damaged bacteria. TEM images were analyzed to determine the percentage of mortality both in controls and treated cells (at the same magnification), by counting a total number of 50,000 cells. Data were collected at different times (0, 10 and 180 min in) and only cells with completely fragmented membranes were considered. Numerical results are presented as mean ± SD. The level for accepted statistical significance was $P < 0.01$. Significantly different ($P < 0.01$) from: (*a*) peptide 0 min, (b) control 0 min, (c) control 10 min, and (d) control 180 min.

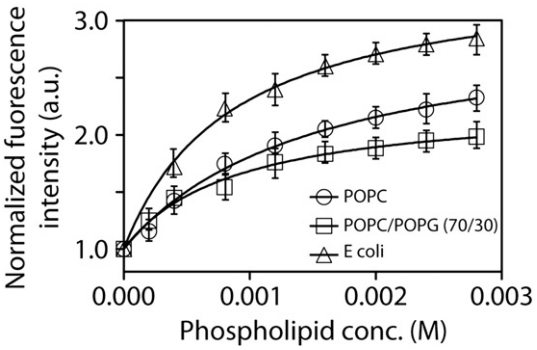

Fig. 5. Binding isotherms for Cnd upon addition of increasing amount of lipid vesicles. The concentration of peptide was 10.0 μM.

(Fig. 2B). A large number of spherical structures, resembling the outer membrane vesicles (OMVs) of Gram-negative bacteria, were found in the extracellular matter, mainly interspersed among cells. A process of bulging out and pinching off of a portion of the bacterial OM, which plays a dynamic role in the formation of OMVs, was noticed in many cells (Fig. 2A; C). The formation of OMVs is a common feature of cold-adapted bacteria that utilize these extracellular vesicles for sensing nutrients [36].

Compared to control, treatment of *Psychrobacter* sp. TAD1 bacteria with the Cnd peptide (10–80 min) induced a significant increase ($P < 0.01$) of the number of cells with membrane damage (Fig. 3).

After 10 min of treatment Cnd perforated both OMs and IMs, with the consequent loss of intracellular components (Figs. 2D and E). Interestingly, this process is localized in well-defined areas, suggesting the formation of well-defined pores (Fig. 2E). After 180 min of treatment we observed no further increase of damaged bacteria (Fig. 3). Cnd also damaged the cell membranes of dividing cells, with leakage of cellular contents and breakup of the basic cellular structure (Fig. 2F). In the extracellular matter were observed fragments of destroyed cellular membranes, whose contents were lacking (Fig. 2G). The morphology of the cellular damage and the time course of the process suggest that Cnd might aggregate on the cell surface, forming well-defined pores together with membrane fragmentation. Discrete pores have been observed for the antimicrobial peptide piscidin-1 [5].

3.2. Outer membrane permeability assay

To compare the ability of Cnd to damage the integrity of the outer membrane of *Psychrobacter* sp. *TDA1* and *E. coli* bacteria, we used the ANS (1-aminonaphtalene-8-sulfonic acid) fluorescence assay [22]. Because of its hydrophobic nature, ANS is not able to pass the cell wall of either *Psychrobacter* sp. *TAD1* or *E. coli*, giving rise to a weak fluorescence signal caused by the high polarity of water. Upon titration of the bacteria cells with Cnd, ANS penetrates the cell membranes, causing a drastic increase of its fluorescence accompanied by a blue shift of the band (Fig. 4). This dose-dependent effect is notable at concentrations as low as 1 μM for both *Psychrobacter* sp. and *E. coli* bacteria, confirming our previous data from the antibacterial activity assays [4].

3.3. Membrane partition of the chionodracine peptide

To quantify the interaction of Cnd with membrane mimetic systems and assess the effects of lipid charges, we measured the fluorescence emission of Tyr-6 of Cnd upon partitioning within membranes of different compositions. Fig. 5 shows the binding isotherms for Cnd upon addition of increasing amount of lipid vesicles.

The mole fraction partition coefficients K_x obtained from the curves ranging from 3×10^4 to 2×10^5 are reported in Table 1. The calculated Gibbs free energies of the water/bilayer partition are −25.6 kJ/mol for pure POPC, −26.5 kJ/mol for the POPC/POPG mixture, and −29.9 kJ/mol for the *E. coli* lipid extract. From these data, it is possible to see a small but significant increase of K_x value using the POPC:POPG mixture. The higher propensity to partition in native *E. coli* lipid extract can be explained by both charge effects and other constituents such as phosphatidylethanolamine (67% wt/wt) and cardiolipin that may anchor the peptide to the membrane. Analogous results have been reported by Vogel and co-workers for indolicin and tritrpticin in interaction with model and natural membranes [37].

3.4. Calcein release studies

Membrane permeabilization by Cnd was also studied by monitoring the increase of calcein fluorescence upon addition of peptide. As calcein has excitation and emission wavelengths of 490 nm and 520 nm, respectively, its leakage from POPC, POPC/POPG (70/30 wt/wt) and *E. coli* extract LUVs was measured as a function of time at different peptide concentrations ranging from 0.1 to 1.0 μM. When a high concentration of calcein is present in the LUVs, the fluorescence is self-quenched. After addition of Cnd to the calcein-loaded vesicles, a gradual release of

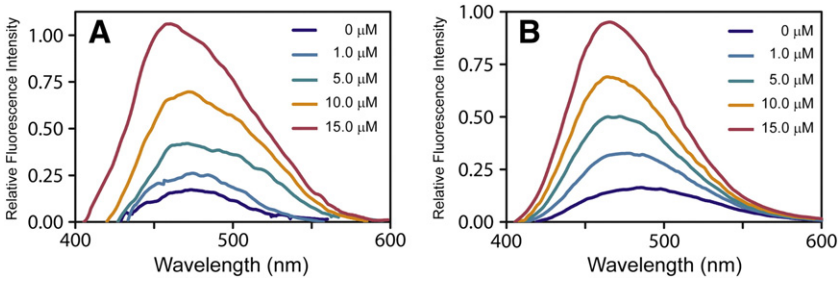

Fig. 4. Permeabilization of *E. coli* (A) and TAD1 (B) outer membrane by Cnd. Fluorescence of ANS equilibrated with cells and in the presence of increasing amount of Cnd peptide from 1.0 through 15 μM. The cell density measured at OD_{600} was 1.2.

Table 1
Partition parameters for Cnd in the presence of different mixtures of POPC/POPG and *E. coli* total lipid extract.

Peptide concentration	Lipid composition	K_x	ΔG (kJ/mol)
1.0 μM	POPC	$(3.43 \pm 0.26) \times 10^4$	−25.9
	POPC/POPG (70/30 w/w)	$(4.91 \pm 0.29) \times 10^4$	−26.7
	Total *E. coli* extract	$(1.83 \pm 0.08) \times 10^5$	−30.0

Table 2
Relative leakage capabilities of Cnd, at different peptide/lipid ratios, in the presence of 100% POPC, 70/30 POPC/POPG and 100% total *E. coli* lipid extract LUVs.

Peptide/lipid (molar ratio)	Relative leakage PC LUVs	Relative leakage POPC/POPG (70/30) LUVs	Relative leakage *E. coli* total extract LUVs
1/25	63%	100%	18%
1/50	26%	90%	13%
1/100	11%	60%	9%

calcein induced by the peptide/lipid bilayers interaction is observed. To confirm that calcein release was due to vesicle/peptide interaction and not to vesicle rupture, the integrity of the lipid vesicles was determined by right angle light scattering. In Table 2, the relative leakage capabilities of Cnd with different liposome vesicles are reported as function of lipid/peptide ratio. We employed POPC vesicles, negatively charged vesicles containing POPC/POPG (70/30 w/w) to simulate bacterial cell membranes, and *E. coli* extract vesicles. The relative percentage of leakage shows that the dose-response of Cnd-induced calcein leakage is more effective in the presence of negatively charged membranes, especially at a low peptide/lipid ratio. The minor leakage capability observed for *E. coli* lipid extract was also reported by Vogel et al. [37] for tryptophan rich cathelicidin antimicrobial peptides; this was attributed to the complexity of the *E. coli* extract making vesicles less prone to disruption.

We also examined the kinetics of leakage using a method developed by Tatulian and co-workers [23]. Fig. 6 shows the fractional release of calcein from a solution containing 25 μM of POPC/POPG vesicles as an example of peptide-induced calcein release. Upon addition of the peptide, a gradual increase of fluorescence due to calcein release is observed until fluorescence reaches the equilibrium, F_{eq}.

The values of the kinetic parameters accounting for the fast and the slow components of the process are reported in Table S1. The kinetic constants depend on the membrane charge and peptide concentrations and range from 0.2–2.0 min and 7–59 min for the fast and the slow components.

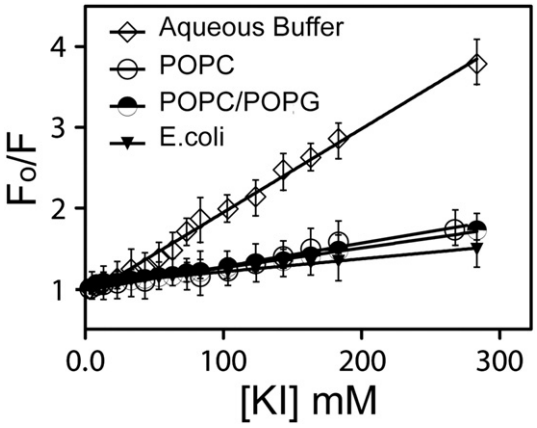

Fig. 7. Stern–Volmer plots for the quenching of Tyrosine 6 of Cnd by KI in aqueous buffer and in the presence of POPC, POPC/POPG (70/30) and *E. coli* total extract LUVs.

3.5. Fluorescence quenching experiments

The degree of peptide exposure to the bulk solvent was assessed through Tyr-6 fluorescence quenching experiments using iodide ions as a quencher [25]. Fig. 7 shows the Stern–Volmer plots for iodide quenching of Cnd in the absence and presence of POPC, POPC/POPG and *E. coli* extract.

The data are corrected for both dilution and absorption of fluorophores. The iodide quenching curves follow a linear correlation with the KI concentration, indicative of collisional quenching. The K_{SV} values, obtained from the slopes of the curves and accounting for the dynamic quenching, are reported in Table 3.

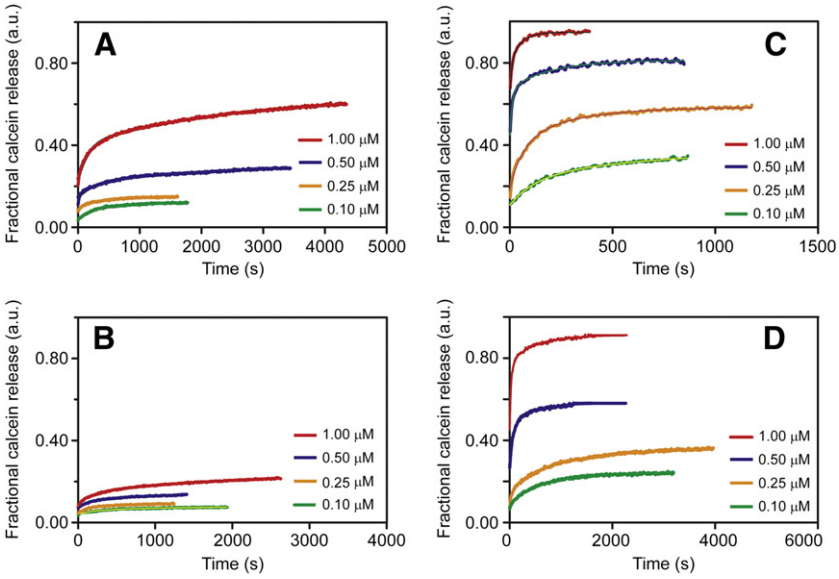

Fig. 6. Kinetics of calcein efflux from LUVs after addition of different amount of Cnd from 0.10 μM through 1.0 μM. The curves are the experimental data normalized by Triton X-100. A) Kinetics curves for POPC LUVs (25.0 μM) at different peptide concentrations; B) kinetics curves for POPC LUVs (50.0 μM); C) kinetics curves for POPC/POPG (70/30) LUVs (25.0 μM) and D) kinetics curves for POPC/POPG (70/30) LUVs (50.0 μM). Note the difference in time scale for different panels.

Table 3
KI quenching. Stern–Volmer quenching constant (K_{SV}) and percentage of iodide quenching for Cnd in the presence of different lipid vesicles. The peptide/lipid molar ratio was 1:100 in all cases.

	K_{SV} (M^{-1})	$1/K_{SV}$ (M)	Percent of quenching
Buffer	10.4 ± 0.2	0.096	100
POPC (LUVs)	2.9 ± 0.1	0.340	28.4
POPC–POPG (70:30 LUVs)	2.5 ± 0.1	0.408	23.6
E. coli (LUVs)	1.6 ± 0.2	0.625	15.4

As expected, the K_{SV} values of are higher in buffer solution ($K_{SV} \approx 10\ M^{-1}$) than in the presence of vesicles ($K_{SV} \approx 3\ M^{-1}$), with the slopes determined in the presence of vesicles ~3–6 fold smaller than in buffer only. This implies that Tyr-6 has a higher accessibility to solvent in the absence of lipid membranes, and suggests that Tyr-6 partitions at the interfacial region of the lipid bilayer. As for the partition constant, the quenching experiments show that the peptide interacts more strongly with charged lipids and with native *E. coli* membranes than with POPC.

3.6. NMR studies of chionodracine in micelles

For the structural studies, Cnd was reconstituted in DPC micelles [38–40]. Sequence specific resonance assignments were obtained by a combination of 2D [^{1}H–^{1}H]-TOCSY and [^{1}H–^{1}H]-NOESY spectra. From these spectra, we assigned most of the resonances and NOE connectivities. Due to slow tumbling of the peptide in micelles, we were not able to measure the *J* coupling constants [38–41]. The complete resonance assignment is given in Table S2. In the TOCSY experiment, we were able to assign most of the fingerprint region containing H_α–H_N cross-peaks. However, only a few spin systems show correlations between the amide and the side chains due to the inefficient relay of magnetization. The peptide spin system assignment was achieved following the NOESY-walk method reported by Wuthrich [32]. From the analysis of the NOESY spectra at 300 ms, a total of 240 NOEs (75 intra-residue and 165 inter-residue) were assigned. Fig. S3 shows the summary of NMR data and NOEs connectivities obtained for the fingerprint region H_α–H_N, the backbone NOE patterns, and the chemical shift index for H_α [42]. We assigned several d_{NN} (i,i + 1) and $d_{\alpha N}$ (i,i + 1) along the peptide backbone, as well as $d_{\alpha N}$ (i,i + 2). Connectivities diagnostic of an α-helical conformation, such as $d_{\alpha N}$ (i,i + 3), $d_{\alpha N}$ (i,i + 4), d_{NN} (i,i + 3) and $d_{\alpha\beta}$ (i,i + 3), were detected along the entire peptide backbone, especially in the region between residues 5 and 20. From the analysis of the natural abundance ^{13}C-edited HSQC, we were able to resolve the amino acid spin system and assign C_α and C_β for the different residues. NMR chemical shifts are strongly related to the secondary structure of proteins and peptides and can be used to calculate the structures [42,43]. To obtain Cnd peptide backbone torsion angles, we input the chemical shifts into TALOS+ [33]. Fig. S4 C reports the RCI-S^2, Random Coil Index derived order parameter S^2 [43], predicting protein flexibility, and the ANN-predicted secondary structure calculated from backbone chemical shifts of H_α, H_N, C_α and C_β using TALOS+ [33]. According to this method, RCI-S^2 values less than 0.5 indicate dynamic residues. In Fig. S4, the bar length is proportional to the probability of the residues to be in either a helix (negative values) or beta-sheet (positive values) conformation. For the Cnd peptide, the average order parameter for residues 5–20 is ~0.8, except for the C-terminal region, which is predicted to be disordered. The conformers obtained from the XPLOR-NIH calculations [34] confirmed this prediction. Fig. 8 displays the superposition of the 40 lowest energy conformers obtained from the structure calculations as well as the average structure. As shown in Fig. 8, the well-defined ensemble is arranged in an α-helical conformation between residues 5 through 20, featuring a classical amphipathic α-helix.

The superposition of backbone atoms between residues H4 through L20 gives a RMSD of 0.30 ± 0.17 Å, and a RMSD of 0.92 ± 0.28 Å for the heavy atoms. From the analysis of the amphipathic helix, there is evidence that hydrophobic residues are on the face of the peptide that is likely closest to the lipid bilayer. The statistics for the 40 best NMR structures of Cnd in DPC micelles are reported in Table S3.

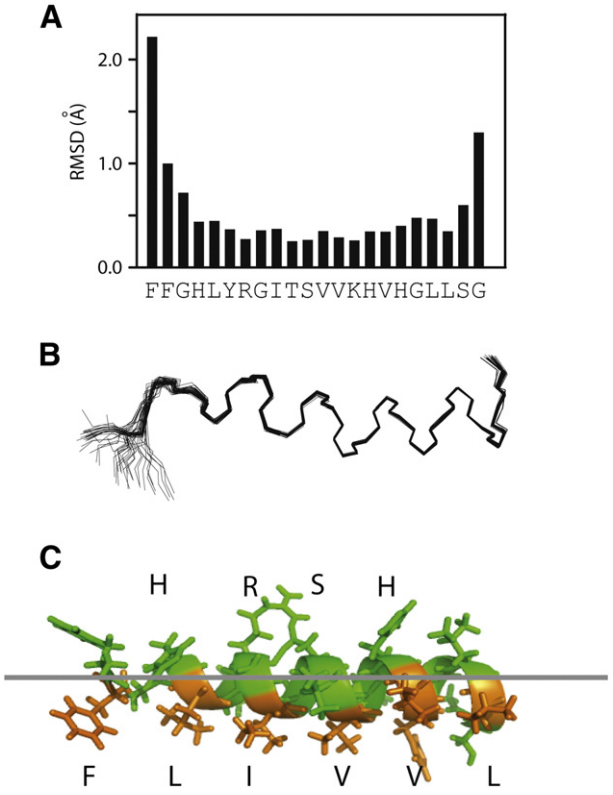

Fig. 8. NMR structural models of Cnd. A) Histogram of the backbone RMSD versus residues for the final 40 Cnd conformers, superimposing heavy atoms for residues 2–20; B) conformational ensemble showing the convergence of the structures for heavy atoms of the backbone; C) representative structure of Cnd showing the two faces of the amphipathic helix. The hydrophilic residues are represented in orange and the hydrophobic residues in green.

4. Discussion and conclusion

Interest in studying AMPs has grown significantly in recent years due to the fact that increasing bacterial resistance to conventional antibiotics is becoming a global emergency [44,45]. The majority of AMPs share the ability to kill a broad spectrum of prokaryotic cells by interacting with and disrupting bacterial cell membranes [46–49]. In addition, several AMPs are involved in modulating immune and inflammatory responses [50,51]. AMPs' broad spectrum of activity, as well as the obstacles they present to the development of resistance, makes them an important candidate for a valid alternative to conventional antibiotics [52]. In fact, some AMPs are already used, in drug formulation, to topically treat infections [45]. Recent studies, reviewed by Hancock, show that AMPs also have immunomodulatory properties [51].

Generally, AMPs such as piscidins are cationic, small (15–45 residues), and amphipathic, with about 50% of their residues hydrophobic to facilitate the interaction with cell membranes [53,54]. Since the first antimicrobial peptide, nisin was isolated in 1947, more than 1800 AMPs have been identified, some natively expressed and others synthesized and tested against different microorganisms [55]. Unfortunately, a unified mechanism of action of AMPs has not yet been found. The only way to understand their biological function is to combine functional assays with detailed structural studies [38–40,56,57].

Peptides derived from fish are attracting growing attention, as they are active at high salt concentrations and a wide range of temperatures, making them ideal candidates for antimicrobial drugs. Pardaxin

from Moses sole (*Pardachirus marmoratus*) was the first fish antimicrobial peptide to be discovered and characterized [38,58]. Thereafter, many peptides showing a broad-spectrum of antimicrobial activity were isolated from fish, such as misgurin from the loach *Misgurnus anguillicaudatus* [59], pleurocidin from winter flounder (*Pleuronectes americanus*) [60], and piscidins from hybrid striped bass (*Morone chrysops* female and *Morone saxatilis* male) [9].

The TEM images show the formation of distinct pores (35–50 nm in diameter), highly localized at possible points of peptide aggregation. This mode of permeabilization supports the macroscopic current and single-channel measurements carried out by Campagna and co-workers on piscidin-1 [5], supporting the formation of discrete pores. Moreover the presence of completely fragmented membranes suggests a carpet-like mechanism of action for Cnd. However Cotten and co-workers emphasize for piscidins 1 and 3 that is difficult to discern between these two mechanism suggesting the carpe model as an extension of pore mechanism [61]. The affinity for synthetic bilayers, quantified via the intrinsic fluorescence quantum yield of the native Tyr 6 of Cnd, shows that the peptide has a piscidin-like behavior with the cationic residues preferentially targeting negative charged lipid membranes. As with the other piscidins, Cnd undergoes a disorder-to-order transition into a well-defined amphipathic α-helical conformation. The amphipathic α-helix motif is a relevant and well-known membrane-binding motif in which both hydrophilic and hydrophobic sites are involved in membrane binding. For instance, an amphipathic helix form from residue 2 through 22 has also been found for the 22 residue analog peptide piscidin 1 in SDS micelles [62]. The presence of an amphipathic helix for the analogues piscidin 1 and piscidin 3 has been confirmed by ssNMR studies in lipid bilayer [61,63,64]. Using ssNMR spectroscopy and MD simulation, Cotten and co-workers [61] showed that piscidin 1 and piscidin 3 insert and rotate in the bilayer; furthermore, due to the presence of the aromatic residues at the N-terminus, it is more deeply inserted in the bilayer than the C-terminus. For Cnd, NMR derived structures (Fig. 8) indicated that Cnd interacts with the lipid membrane so that the non-polar face is in contact with the hydrophobic portion of the membrane and the polar residues are oriented toward the solvent [65]. This evidence is also confirmed by the Tyr-6 quenching studies. As reported in Table 3, Tyr 6 is much less accessible to the solvent upon binding with lipid vesicles, and the Stern–Volmer constant is 3–6 fold smaller, depending on the vesicles, than in buffer. The decrease in accessibility of the fluorophore to the quencher can be explained by the fact that, upon binding, the N-terminus is deeply inserted into the lipid bilayer due to the presence of the two phenylalanine residues in positions 1 and 2. Moreover, the presence of anionic lipids lowers the Gibbs partition energy by about 4 kJ/mol moving from the zwitterionic POPC to the anionic mixture (POPC/POPG 70:30). We speculate that following binding to the membrane surface, there is a perturbation of the lipid membrane and the formation of pores and membrane fragmentation that concur to the leakage of the cell content. To this extent, leakage measurements reveal the ability of Cnd to induce calcein release from lipid vesicles in a dose-dependent manner, based on both peptide-to-lipid ratio as well as the type of lipids used (Fig. 4). The efflux rates increase in the presence of a higher peptide/lipid ratio and in the presence of anionic lipids, likely as a consequence of better binding, as confirmed by higher values of K_x. At low peptide to lipid ratios the induced leakage is low, while upon increasing this ratio the leakage also drastically increases [24].

In conclusion, the combination of TEM, fluorescence data, solution NMR spectroscopy, and lipid binding assays of Cnd support a mechanism of action in which the mature peptide is essentially unstructured and adopts a canonical α-helical structure upon interaction with lipid membranes, with a preference toward charged lipids and *E. coli* extracts. The TEM images and the NMR data suggest that the initial adsorption of the peptide on membranes is followed by the recruiting of other monomers, forming well-defined pores that perforate both inner and outer membranes. The latter mechanism occurs together with an extensive membrane fragmentation that concurs to killing bacterial cells. Given the weak hemolytic activity of Cnd, these data suggest that this peptide could constitute a great starting point for the development of more specific and potent antimicrobial agents.

Transparency document

The Transparency document associated with this article can be found, in the online version.

Appendix A. Supplementary data

Supplementary data to this article can be found online at http://dx.doi.org/10.1016/j.bbamem.2015.02.030.

References

[1] H.G. Boman, Antibacterial peptides: basic facts and emerging concepts, J. Intern. Med. 254 (2003) 197–215.
[2] F. Porcelli, A. Ramamoorthy, G. Barany, G. Veglia, On the role of NMR spectroscopy for characterization of antimicrobial peptides, Methods Mol. Biol. 1063 (2013) 159–180.
[3] A. Izadpanah, R.L. Gallo, Antimicrobial peptides, J. Am. Acad. Dermatol. 52 (2005) 381–390.
[4] F. Buonocore, E. Randelli, D. Casani, S. Picchietti, M.C. Belardinelli, D. de Pascale, C. De Santi, G. Scapigliati, A piscidin-like antimicrobial peptide from the icefish *Chionodraco hamatus* (Perciformes: Channichthyidae) molecular characterization, localization and bactericidal activity, Fish Shellfish Immunol. 33 (2012) 1183–1191.
[5] S. Campagna, N. Saint, G. Molle, A. Aumelas, Structure and mechanism of action of the antimicrobial peptide piscidin, Biochemistry 46 (2007) 1771–1778.
[6] J.A. Masso-Silva, G. Diamond, Antimicrobial peptides from fish, Pharmaceuticals (Basel) 7 (2014) 265–310.
[7] W.S. Sung, J. Lee, D.G. Lee, Fungicidal effect and the mode of action of piscidin 2 derived from hybrid striped bass, Biochem. Biophys. Res. Commun. 371 (2008) 551–555.
[8] W.J. Lin, Y.L. Chien, C.Y. Pan, T.L. Lin, J.Y. Chen, S.J. Chiu, C.F. Hui, Epinecidin-1, an antimicrobial peptide from fish (*Epinephelus coioides*) which has an antitumor effect like lytic peptides in human fibrosarcoma cells, Peptides 30 (2009) 283–290.
[9] E.J. Noga, U. Silphaduang, Piscidins: a novel family of peptide antibiotics from fish, Drug News Perspect. 16 (2003) 87–92.
[10] B. Bechinger, P.M. Macdonald, J. Seelig, Deuterium NMR studies of the interactions of polyhydroxyl compounds and of glycolipids with lipid model membranes, Biochim. Biophys. Acta 943 (1988) 381–385.
[11] J.C. Hsu, L.C. Lin, J.T. Tzen, J.Y. Chen, Characteristics of the antitumor activities in tumor cells and modulation of the inflammatory response in RAW264.7 cells of a novel antimicrobial peptide, chrysophsin-1, from the red sea bream (Chrysophrys major), Peptides 32 (2011) 900–910.
[12] A.L. Hilchie, C.D. Doucette, D.M. Pinto, A. Patrzykat, S. Douglas, D.W. Hoskin, Pleurocidin-family cationic antimicrobial peptides are cytolytic for breast carcinoma cells and prevent growth of tumor xenografts, Breast Cancer Res. 13 (2011) R102.
[13] R.E. Hancock, H.G. Sahl, New strategies and compounds for anti-infective treatment, Curr. Opin. Microbiol. 16 (2013) 519–521.
[14] E.F. Nicholls, L. Madera, R.E. Hancock, Immunomodulators as adjuvants for vaccines and antimicrobial therapy, Ann. N. Y. Acad. Sci. 1213 (2010) 46–61.
[15] C. Pujol, E. Eugene, L. DesaintMartin, X. Nassif, Interaction of *Neisseria meningitidis* with a polarized monolayer of epithelial cells, Infect. Immun. 65 (1997) 4836–4842.
[16] A.S. Ladokhin, S. Jayasinghe, S.H. White, How to measure and analyze tryptophan fluorescence in membranes properly, and why bother? Anal. Biochem. 285 (2000) 235–245.
[17] W.C. Wimley, S.H. White, Membrane partitioning: distinguishing bilayer effects from the hydrophobic effect, Biochemistry 32 (1993) 6307–6312.
[18] M. Fernández-Vidal, S.H. White, A.S. Ladokhin, Membrane partitioning: "classical" and "nonclassical" hydrophobic effects, J. Membr. Biol. 239 (2011) 5–14.
[19] r. rathinakumar, w.c. wimley, Biomolecular engineering by combinatorial design and high-throughput screening: small, soluble peptides that permeabilize membranes, J. Am. Chem. Soc. 130 (2008) 9849–9858.
[20] A.S. Ladokhin, Fluorescence spectroscopy in thermodynamic and kinetic analysis of pH-dependent membrane protein insertion, Methods Enzymol. 466 (2009) 19–42.
[21] S.H. White, W.C. Wimley, A.S. Ladokhin, K. Hristova, Protein folding in membranes: determining energetics of peptide-bilayer interactions, Methods Enzymol. 295 (1998) 62–87.
[22] P.N. Domadia, A. Bhunia, A. Ramamoorthy, S. Bhattacharjya, Structure, interactions, and antibacterial activities of MSI-594 derived mutant peptide MSI-594F5A in lipopolysaccharide micelles: role of the helical hairpin conformation in outer-membrane permeabilization, J. Am. Chem. Soc. 132 (2010) 18417–18428.
[23] P. Garg, K.N. Nemec, A.R. Khaled, S.A. Tatulian, Transmembrane pore formation by the carboxyl terminus of Bax protein, Biochim. Biophys. Acta 1828 (2013) 732–742.
[24] N.G. Park, U. Silphaduang, H.S. Moon, J.K. Seo, J. Corrales, E.J. Noga, Structure-activity relationships of piscidin 4, a piscine antimicrobial peptide, Biochemistry 50 (2011) 3288–3299.
[25] J.R. Lackowicz, Principle of Fluorescence Spectroscopy, 2006.

[26] A.D. Bax, D.G. Davis, MLEV-17-based two-dimensional homonuclear magnetization transfer spectroscopy, J. Magn. Reson. 65 (1985) (1969) 355–360.
[27] A. Kumar, R.R. Ernst, K. Wüthrich, A two-dimensional nuclear overhauser enhancement (2D NOE) experiment for the elucidation of complete proton–proton cross-relaxation networks in biological macromolecules, Biochem. Biophys. Res. Commun. 95 (1980) 1–6.
[28] M. Piotto, V. Saudek, V. SklenáŘ, Gradient-tailored excitation for single-quantum NMR spectroscopy of aqueous solutions, J. Biomol. NMR 2 (1992) 661–665.
[29] A.J. Shaka, C.J. Lee, A. Pines, Iterative schemes for bilinear operators; application to spin decoupling, J. Magn. Reson. 77 (1988) (1969) 274–293.
[30] F. Delaglio, S. Grzesiek, G.W. Vuister, G. Zhu, J. Pfeifer, A.D. Bax, NMRPipe: a multidimensional spectral processing system based on UNIX pipes, J. Biomol. NMR 6 (1995) 277–293.
[31] T.D. Goddard, D.G. Kneller, SPARKY 3, 14University of California, San Francisco, 2004. 15.
[32] K. Wuthrich, NMR of proteins and nucleic acids, Wiley, 1986.
[33] Y. Shen, F. Delaglio, G. Cornilescu, A. Bax, TALOS+: a hybrid method for predicting protein backbone torsion angles from NMR chemical shifts, J. Biomol. NMR 44 (2009) 213–223.
[34] C.D. Schwieters, J.J. Kuszewski, G. Marius Clore, Using Xplor-NIH for NMR molecular structure determination, Prog. Nucl. Magn. Reson. Spectrosc. 48 (2006) 47–62.
[35] I.W. Davis, A. Leaver-Fay, V.B. Chen, J.N. Block, G.J. Kapral, X. Wang, L.W. Murray, W.B. Arendall 3rd, J. Snoeyink, J.S. Richardson, D.C. Richardson, MolProbity: all-atom contacts and structure validation for proteins and nucleic acids, Nucleic Acids Res. 35 (2007) W375–W383.
[36] A. Frias, A. Manresa, E. de Oliveira, C. Lopez-Iglesias, E. Mercade, Membrane vesicles: a common feature in the extracellular matter of cold-adapted Antarctic bacteria, Microb. Ecol. 59 (2010) 476–486.
[37] V.V. Andrushchenko, M.H. Aarabi, L.T. Nguyen, E.J. Prenner, H.J. Vogel, Thermodynamics of the interactions of tryptophan-rich cathelicidin antimicrobial peptides with model and natural membranes, Biochim. Biophys. Acta Biomembr. 1778 (2008) 1004–1014.
[38] F. Porcelli, B. Buck, D.-K. Lee, K.J. Hallock, A. Ramamoorthy, G. Veglia, Structure and orientation of pardaxin determined by NMR experiments in model membranes, J. Biol. Chem. 279 (2004) 45815–45823.
[39] F. Porcelli, B.A. Buck-Koehntop, S. Thennarasu, A. Ramamoorthy, G. Veglia, Structures of the dimeric and monomeric variants of magainin antimicrobial peptides (MSI-78 and MSI-594) in micelles and bilayers, determined by NMR spectroscopy, Biochemistry 45 (2006) 5793–5799.
[40] F. Porcelli, R. Verardi, L. Shi, K.A. Henzler-Wildman, A. Ramamoorthy, G. Veglia, NMR structure of the cathelicidin-derived human antimicrobial peptide LL-37 in dodecylphosphocholine micelles†, Biochemistry 47 (2008) 5565–5572.
[41] A. Mascioni, F. Porcelli, U. Ilangovan, A. Ramamoorthy, G. Veglia, Conformational preferences of the amylin nucleation site in SDS micelles: an NMR study, Biopolymers 69 (2003) 29–41.
[42] D.S. Wishart, B.D. Sykes, F.M. Richards, The chemical shift index: a fast and simple method for the assignment of protein secondary structure through NMR spectroscopy, Biochemistry 31 (1992) 1647–1651.
[43] M.V. Berjanskii, D.S. Wishart, Application of the random coil index to studying protein flexibility, J. Biomol. NMR 40 (2008) 31–48.
[44] W.C. Wimley, K. Hristova, Antimicrobial peptides: successes, challenges and unanswered questions, J. Membr. Biol. 239 (2011) 27–34.
[45] G. Roscia, C. Falciani, L. Bracci, A. Pini, The development of antimicrobial peptides as new antibacterial drugs, Curr. Protein Pept. Sci. 14 (2013) 641–649.
[46] J.P. Powers, R.E. Hancock, The relationship between peptide structure and antibacterial activity, Peptides 24 (2003) 1681–1691.
[47] K.A. Brogden, Antimicrobial peptides: pore formers or metabolic inhibitors in bacteria? Nat. Rev. Microbiol. 3 (2005) 238–250.
[48] E. Jamasbi, S. Batinovic, R.A. Sharples, M.A. Sani, R.M. Robins-Browne, J.D. Wade, F. Separovic, M.A. Hossain, Melittin peptides exhibit different activity on different cells and model membranes, Amino Acids 46 (2014) 2759–2766.
[49] D.I. Fernandez, A.P. Le Brun, T.C. Whitwell, M.A. Sani, M. James, F. Separovic, The antimicrobial peptide aurein 1.2 disrupts model membranes via the carpet mechanism, Phys. Chem. Chem. Phys. 14 (2012) 15739–15751.
[50] Y. Lai, R.L. Gallo, AMPed up immunity: how antimicrobial peptides have multiple roles in immune defense, Trends Immunol. 30 (2009) 131–141.
[51] A.L. Hilchie, K. Wuerth, R.E. Hancock, Immune modulation by multifaceted cationic host defense (antimicrobial) peptides, Nat. Chem. Biol. 9 (2013) 761–768.
[52] M. Vaara, New approaches in peptide antibiotics, Curr. Opin. Pharmacol. 9 (2009) 571–576.
[53] B. Bechinger, E.S. Salnikov, The membrane interactions of antimicrobial peptides revealed by solid-state NMR spectroscopy, Chem. Phys. Lipids 165 (3) (2012) 282–301.
[54] R.M. Verly, C.M. de Moraes, J.M. Resende, C. Aisenbrey, M.P. Bemquerer, D. Pilo-Veloso, A.P. Valente, F.C. Almeida, B. Bechinger, Structure and membrane interactions of the antibiotic peptide dermadistinctin K by multidimensional solution and oriented 15 N and 31P solid-state NMR spectroscopy, Biophys. J. 96 (2009) 2194–2203.
[55] G. Wang, X. Li, Z. Wang, APD2: the updated antimicrobial peptide database and its application in peptide design, Nucleic Acids Res. 37 (2009) D933–D937.
[56] R. Verardi, N.J. Traaseth, L. Shi, F. Porcelli, L. Monfregola, S. De Luca, P. Amodeo, G. Veglia, A. Scaloni, Probing membrane topology of the antimicrobial peptide distinctin by solid-state NMR spectroscopy in zwitterionic and charged lipid bilayers, Biochim. Biophys. Acta 1808 (2011) 34–40.
[57] S.T. Henriques, D.J. Craik, Importance of the cell membrane on the mechanism of action of cyclotides, ACS Chem. Biol. 7 (2012) 626–636.
[58] N. Primor, P. Lazarovici, *Pardachirus marmoratus* (Red Sea flatfish) secretion and its isolated toxic fraction pardaxin: the relationship between hemolysis and ATPase inhibition, Toxicon 19 (1981) 573–578.
[59] S. Yan, G. Wu, Analysis on folding of misgurin using two-dimensional HP model, Proteins 80 (2012) 764–773.
[60] P. Pundir, A. Catalli, C. Leggiadro, S.E. Douglas, M. Kulka, Pleurocidin, a novel antimicrobial peptide, induces human mast cell activation through the FPRL1 receptor, Mucosal Immunol. 7 (2014) 177–187.
[61] B.S. Perrin, Y. Tian, R. Fu, C.V. Grant, E.Y. Chekmenev, W.E. Wieczorek, A.E. Dao, R.M. Hayden, C.M. Burzynski, R.M. Venable, M. Sharma, S.J. Opella, R.W. Pastor, M.L. Cotten, High-resolution structures and orientations of antimicrobial peptides piscidin 1 and piscidin 3 in fluid bilayers reveal tilting, kinking, and bilayer immersion, J. Am. Chem. Soc. 136 (2014) 3491–3504.
[62] S.-A. Lee, Y.K. Kim, S.S. Lim, W.L. Zhu, H. Ko, S.Y. Shin, K.-S. Hahm, Y. Kim, Solution structure and cell selectivity of piscidin 1 and its analogues, Biochemistry 46 (2007) 3653–3663.
[63] A.A. De Angelis, C.V. Grant, M.K. Baxter, J.A. McGavin, S.J. Opella, M.L. Cotten, Amphipathic antimicrobial piscidin in magnetically aligned lipid bilayers, Biophys. J. 101 (2011) 1086–1094.
[64] R. Fu, E.D. Gordon, D.J. Hibbard, M. Cotten, High resolution heteronuclear correlation NMR spectroscopy of an antimicrobial peptide in aligned lipid bilayers: peptide-water interactions at the water-bilayer interface, J. Am. Chem. Soc. 131 (2009) 10830–10831.
[65] M.R. de Planque, B.B. Bonev, J.A. Demmers, D.V. Greathouse, R.E. Koeppe 2nd, F. Separovic, A. Watts, J.A. Killian, Interfacial anchor properties of tryptophan residues in transmembrane peptides can dominate over hydrophobic matching effects in peptide-lipid interactions, Biochemistry 42 (2003) 5341–5348.